Monthly Notices
of the
ROYAL ASTRONOMICAL SOCIETY

MNRAS **473,** 2679–2687 (2018)
Advance Access publication 2017 October 2

doi:10.1093/mnras/stx2547

SDSS-IV MaNGA: the different quenching histories of fast and slow rotators

R. J. Smethurst,[1]★ K. L. Masters,[2] C. J. Lintott,[3] A. Weijmans,[4] M. Merrifield,[1] S. J. Penny,[2] A. Aragón-Salamanca,[1] J. Brownstein,[5] K. Bundy,[6] N. Drory,[7] D. R. Law[8] and R. C. Nichol[2]

[1]*School of Physics and Astronomy, The University of Nottingham, University Park, Nottingham NG7 2RD, UK*
[2]*Institute of Cosmology and Gravitation, University of Portsmouth, Dennis Sciama Building, Barnaby Road, Portsmouth PO13FX, UK*
[3]*Oxford Astrophysics, Department of Physics, University of Oxford, Denys Wilkinson Building, Keble Road, Oxford OX13RH, UK*
[4]*School of Physics and Astrononomy, University of St Andrews, North Haugh, St Andrews, Fife KY169RJ, UK*
[5]*Department of Physics and Astronomy, University of Utah, 115 S. 1400 E., Salt Lake City, UT 84112, USA*
[6]*University of California, Santa Cruz, 1156 High St. Santa Cruz, CA 95064, USA*
[7]*McDonald Observatory, The University of Texas at Austin, 1 University Station, Austin, TX 78712, USA*
[8]*Space Telescope Science Institute, 3700 San Martin Drive, Baltimore, MD 21218, USA*

Accepted 2017 September 26. Received 2017 September 25; in original form 2017 August 25

ABSTRACT

Do the theorized different formation mechanisms of fast and slow rotators produce an observable difference in their star formation histories? To study this, we identify quenching slow rotators in the MaNGA sample by selecting those that lie below the star-forming sequence and identify a sample of quenching fast rotators that were matched in stellar mass. This results in a total sample of 194 kinematically classified galaxies, which is agnostic to visual morphology. We use $u - r$ and $NUV - u$ colours from the Sloan Digital Sky Survey and *GALEX* and an existing inference package, STARPY, to conduct a first look at the onset time and exponentially declining rate of quenching of these galaxies. An Anderson–Darling test on the distribution of the inferred quenching rates across the two kinematic populations reveals they are statistically distinguishable (3.2σ). We find that fast rotators quench at a much wider range of rates than slow rotators, consistent with a wide variety of physical processes such as secular evolution, minor mergers, gas accretion and environmentally driven mechanisms. Quenching is more likely to occur at rapid rates ($\tau \lesssim 1$ Gyr) for slow rotators, in agreement with theories suggesting slow rotators are formed in dynamically fast processes, such as major mergers. Interestingly, we also find that a subset of the fast rotators quench at these same rapid rates as the bulk of the slow rotator sample. We therefore discuss how the total gas mass of a merger, rather than the merger mass ratio, may decide a galaxy's ultimate kinematic fate.

Key words: galaxies: general – galaxy: photometry – galaxies: statistics.

1 INTRODUCTION

Recent work studying the early-type (i.e. elliptical and lenticular) galaxy population has revealed that it is actually composed of two kinematically distinct populations. The majority of early-types are rotationally supported (Emsellem et al. 2011) with ∼seven times the number of galaxies with kinematic discs ('fast' rotators), compared to those with either dispersion-dominated kinematics ('slow' rotators) or kinematically decoupled cores (which, along with slow rotators, are collectively referred to as 'non-regular' rotators; Cappellari et al. 2007; Emsellem et al. 2007). This has led to the proposal of a revision of Hubble's morphological classification scheme in the form of a 'comb' (see fig. 24 of Cappellari 2016), whereby the evolution of a galaxy, from disc- to bulge-dominated, takes place along a 'tine' of the comb as a fast rotator, always retaining an underlying disc. If the discs of these regular rotators are destroyed, they then evolve along the 'handle' of the comb to become slow rotators.

Dry major mergers are considered the most likely process to produce high stellar mass slow rotators (Bois et al. 2010; Duc et al. 2011; Naab et al. 2014) as they can rapidly destroy the disc-dominated nature of a galaxy (Toomre & Toomre 1972). Low stellar mass slow rotators (i.e. dwarf ellipticals with $M_* \lesssim 10^9\,\mathrm{M}_\odot$) are thought to be formed via harassment mechanisms in the group and cluster environment (Toloba et al. 2015). Fast rotators are thought

★ E-mail: rebecca.smethurst@nottingham.ac.uk

Table 1. Summary of the generalized rates of theorized internal and external quenching mechanisms (see Smethurst et al. 2017).

	Internal processes ('nature')	External processes ('nurture')
Fast quenching	AGN feedback	Mergers
Intermediate quenching	Mass quenching	Environmental quenching
Slow quenching	Morphological quenching	Gas accretion

to evolve from the slow build up of a galaxy's bulge over time, eventually overwhelming the disc. This growth is thought to occur via gas-rich major or minor mergers (Duc et al. 2011) and by gas accretion (Cappellari et al. 2013; Johnston, Aragón-Salamanca & Merrifield 2014), which can produce a bulge-dominated but rotationally supported galaxy (which would be visually classified as an early-type in the Hubble classification scheme).

The possible formation mechanisms listed above are also often proposed as external quenching mechanisms of star formation in a galaxy. However, these mechanisms are not thought to quench a galaxy at the same rate. Dynamically faster processes, such as mergers, are thought to quench star formation at rapid rates (Hopkins et al. 2008; Snyder et al. 2011; Hayward et al. 2014), with major mergers thought to cause a much faster quench of the remnant galaxy than a minor merger (Lotz et al. 2008, 2011). Similarly, environmental processes, such as harassment, are also thought to cause quenching through repeated high speed interactions with neighbouring galaxies. Over time, these interactions can strip both stars and gas from a galaxy and heat the gas needed for star formation (Knebe et al. 2006; Aguerri & González-García 2009), quenching the galaxy at a slower rate than a merger. Slow quenching by an external process is also possible through gas accretion due to the large gravitational potential of the bulge, which builds as the accreted gas sinks to the centre of the galaxy. This prevents the disc from collapsing and forming stars in an internal process, which is categorized as morphological quenching (Martig et al. 2009; Fang et al. 2013). Similarly, there are internal processes that are theorized to cause quenching in galaxies, including active galactic nucleus (AGN) feedback (Croton et al. 2006; Somerville et al. 2008), mass quenching (Peng et al. 2010, 2012) and morphological quenching (e.g. due to a galactic bar, Zurita et al. 2004; Sheth et al. 2005) at rapid, intermediate and slow quenching rates, respectively. Crucially, external quenching processes are the only mechanisms theorized to be able to change the morphology of a galaxy (see section 1 of Smethurst et al. 2017, for a more detailed introduction to possible quenching mechanisms). These quenching mechanisms and their theorized rates are summarized in Table 1.

If fast and slow rotators form via different mechanisms, we should therefore also expect to find a difference in the star formation histories of quenching or quenched fast and slow rotators. This paper presents a first look at this problem by using an existing Bayesian star formation inference package, STARPY, to determine the quenching histories of a sample of quenching or quenched fast and slow rotators identified in the MaNGA sample, irrespective of visual morphology. We use broad-band optical, $u - r$, and near-ultraviolet, $NUV - u$, colours from the Sloan Digital Sky Survey (SDSS) and *GALEX* to infer both the onset time and exponential rate of quenching for each galaxy. We aim to determine whether kinematically distinct galaxies have different quenching histories.

This paper proceeds as follows. In Section 2, we describe our data sources and our Bayesian inference method for determining the quenching histories. We present our results in Section 3 and discuss the implications of these results in Section 4. The zero-points of all magnitudes are in the AB system. We adopt the WMAP Seven-Year Cosmology (Jarosik et al. 2011) with $(\Omega_m,\ \Omega_\Lambda,\ h) = (0.26, 0.73, 0.71)$.

2 DATA AND METHODS

2.1 SDSS and *GALEX* Photometry

We use optical photometry from the Sloan Digital Sky Survey Data Release 7 (SDSS DR7; York et al. 2000; Abazajian et al. 2009). We use the Petrosian magnitude, `petroMag`, values for the u (3543Å) and r (6231Å) wavebands provided by the SDSS DR7 pipeline (Stoughton et al. 2002). Further to this, we also required *NUV* (2267Å) photometry from the *GALEX* survey (Martin et al. 2005). Observed fluxes are corrected for galactic extinction (Oh et al. 2011) by applying the Cardelli, Clayton & Mathis (1989) law. We also adopt k-corrections to $z = 0.0$ and obtain absolute magnitudes from the NYU-VAGC[1] (Blanton et al. 2005; Blanton & Roweis 2007; Padmanabhan et al. 2008).

2.2 MaNGA Survey and data reduction pipeline

MaNGA is a multiobject IFU survey conducted with the 2.5−m Sloan Foundation Telescope (Gunn et al. 2006) at the Apache Point Observatory (APO) as part of SDSS-IV (Blanton et al. 2017). By 2020, MaNGA will have acquired IFU spectroscopy for ∼10 000 galaxies with $M_* > 10^9$ M$_\odot$ and an approximately flat mass selection (Wake et al. 2017). The target selection is agnostic to morphology, colour and environment.

MaNGA makes use of the Baryon Oscillation Spectroscopic Survey (BOSS) spectrograph (Smee et al. 2013). The BOSS spectrograph provides continuous coverage between 3600 and 10 300 Å at a spectral resolution $R \sim 2000$ ($\sigma_{\rm instrument} \sim 77$ km s^{-1} for the majority of the wavelength range[2]).

Complete spectral coverage to $1.5R_e$, a galaxy's effective radius, is obtained for the majority of targets; a subset have coverage to $2.5R_e$. See Bundy et al. (2015) for an overview of the MaNGA survey. For a further description of the instrumentation used by MaNGA, see Drory et al. (2015). For a detailed description of the observing strategy, see Law et al. (2015), and for a description of the survey design, see Yan et al. (2016).

The raw data were processed by the MaNGA data reduction pipeline (DRP version 2.0.1), which is discussed in detail in Law et al. (2016). The MaNGA DRP extracts, wavelength calibrates and flux calibrates all fibre spectra obtained in every exposure. The individual fibre spectra are then used to form a regular gridded data cube of 0.5 arcsec 'spaxels' and spectral channels. The spectra are logarithmically sampled with bin widths of $\log \lambda = 10^{-4}$.

[1] http://sdss.physics.nyu.edu/vagc/

[2] Instrument resolution as a function of wavelength is shown in fig. 20 of Yan et al. (2016).

These data cubes are then analysed using the MaNGA data analysis pipeline (DAP version 2.0.2); the development of which is ongoing and will be described in detail in Westfall et al. (in preparation). Briefly, the spectral emission lines are masked, and the stellar continuum is modelled using the kinematic and stellar population fitting package PPXF (Cappellari & Emsellem 2004). The stellar continuum model is then constructed using a thinned version of the MILES spectral library [wavelength range $3525 < \lambda$ (Å) < 7500]. The model is broadened to match the stellar velocity dispersion of the galaxy in order to cleanly subtract the absorption lines from the spectrum. The residual emission lines are then modelled using Gaussian profiles, with 21 different lines fit in total. The primary output from the DAP are therefore 2D 'maps' (i.e. images) of these measured properties, including flux, stellar and gas kinematics, spectral index measurements, and absorption- and emission-line properties. The effective radius of a galaxy and the ellipticity within it, ϵ_e, are provided for MaNGA galaxies in the NASA Sloan Atlas; we use the values measured with elliptical Petrosian apertures in v1_0_1 of the catalogue provided in the SDSS Data Release 13 (SDSS Collaboration et al. 2016).

2.3 Data sample

Our galaxy sample is drawn from the 2 777 SDSS galaxies, which make up the MaNGA DR14 data release (Abolfathi et al. 2017). We cross-matched these galaxies with a radius of 3 arcsec to the *GALEX* survey in order to obtain *NUV* photometry (see Section 2.1), resulting in 1 413 galaxies.

In this study, we wish to investigate the quenching histories of galaxies, therefore we sub-select those galaxies that are below the star-forming sequence (SFS). Here, we use the global average star formation rates (SFRs) quoted in the MPA-JHU catalogue[3] (Kauffmann et al. 2003; Brinchmann et al. 2004, which are corrected for aperture bias). We do not use the MaNGA spectra to calculate SFRs; since the bundles only extend to $1.5\,R_e$, we might miss star formation occurring in the outer regions of galaxies, which would result in an underestimate of the global SFR of a galaxy.

We select galaxies with an SFR more than 1σ below the SFS of Peng et al. (2010). Since we wish to test whether slow rotators quench at rapid rates, consistent with major mergers, we wish to include those galaxies that have just left the SFS (rather than only selecting those that are fully quenched, for example, 3σ below the SFS).

This selection on SFR when applied to the MANGA-GALEX sample results in a sample of 826 quenching or quenched galaxies, which we will refer to as the Q-MANGA-GALEX sample. This sample is shown in Fig. 1.

2.4 Identifying slow and fast rotators

In order to classify the galaxies in the Q-MANGA-GALEX sample as slow rotators or otherwise, we first calculate the specific stellar angular momentum as defined by Emsellem et al. (2007, 2011);

$$\lambda_{R_e} = \frac{\sum_{i=1}^{N} F_i\, R_i\, |V_i|}{\sum_{i=1}^{N} F_i\, R_i\, (V_i^2 + \sigma_i^2)^{1/2}}, \qquad (1)$$

where F_i is the flux in the ith spaxel, R_i the spaxel's distance from the galaxy centre (where $R_i < R_e$, the effective radius of a galaxy), V_i the mean stellar velocity in that spaxel, σ_i the stellar velocity dispersion in that spaxel and N the total number of spaxels. In this work, we use the PYTHON function provided in the MaNGA DAP to calculate λ_{R_e} using the values of mean flux, radius, stellar velocity and stellar velocity dispersion (corrected for instrumental resolution effects) in each bin of the MaNGA data cubes binned with a signal-to-noise ratio of 10 using a Voronoi binning algorithm (Cappellari & Copin 2003), as calculated by the MaNGA DAP (see Section 2.2). Velocity dispersion measurements in each bin of a galaxy data cube were confirmed to be above the instrument resolution of 77 km s^{-1}.

[3] http://wwwmpa.mpa-garching.mpg.de/SDSS/DR7/

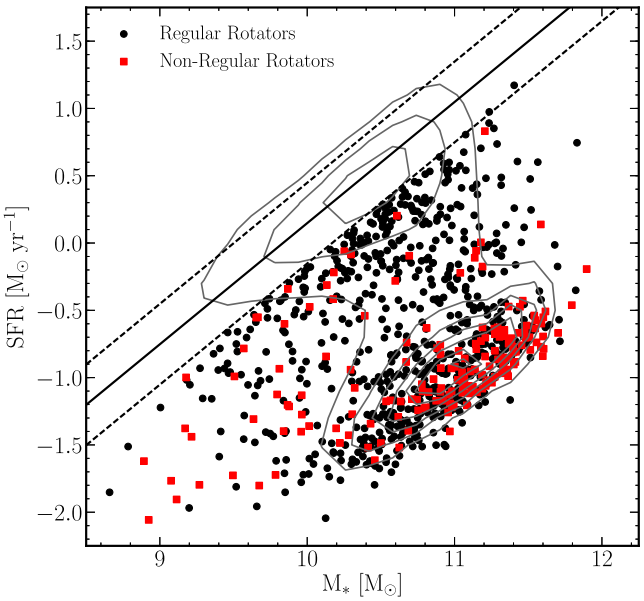

Figure 1. Stellar mass against SFR for the Q-MANGA-GALEX sample with regular (black circles) and non-regular (red squares) rotators identified using equation (2). Shown also are the contours for the entire MPA-JHU sample (grey contours; i.e. SDSS DR7). The solid line shows the SFS as defined by Peng et al. (2010) at the average redshift of the Q-MANGA-GALEX sample, with $\pm 1\sigma$ shown by the dashed lines. Note that the galaxies in the Q-MANGA-GALEX sample are chosen to be more than 1σ below the SFS as defined at their observed redshift and stellar mass (see Section 2.3).

We then classify galaxies in the Q-MANGA-GALEX sample as non-regular rotators, or otherwise, using the definition from Cappellari (2016):

$$\lambda_{R_e} < 0.08 + \frac{\epsilon_e}{4} \quad \text{with} \quad \epsilon_e < 0.4. \qquad (2)$$

Both slow rotators and kinematically disturbed galaxies will satisfy this inequality, hence why this selection results in a sample of non-regular rotators. Using this definition reveals 168 (20 per cent) non-regular rotators and 658 (80 per cent) regular rotators in the Q-MANGA-GALEX sample. Fig. 2 shows the velocity maps of these galaxies plotted at their values of λ_{R_e} and ϵ_e, along with the definition of a non-regular rotator from Cappellari (2016) shown by the solid black line. Note the Q-MANGA-GALEX sample is agnostic to visual morphology, so our sample of regular rotators will contain both rotationally supported early-type and late-type galaxies.

The fraction of non-regular rotators found in the Q-MANGA-GALEX sample (20 per cent) is slightly higher than that found by previous works (14−17 per cent of early-types in the ATLAS^{3D} sample; Emsellem et al. 2011; Stott et al. 2016). However, we must be wary with this comparison since the ATLAS^{3D} sample is volume limited, whereas the MaNGA sample is selected to have a flat stellar mass distribution, prior to our selection on *GALEX* cross-matches and those galaxies below the SFS. Therefore, although a direct

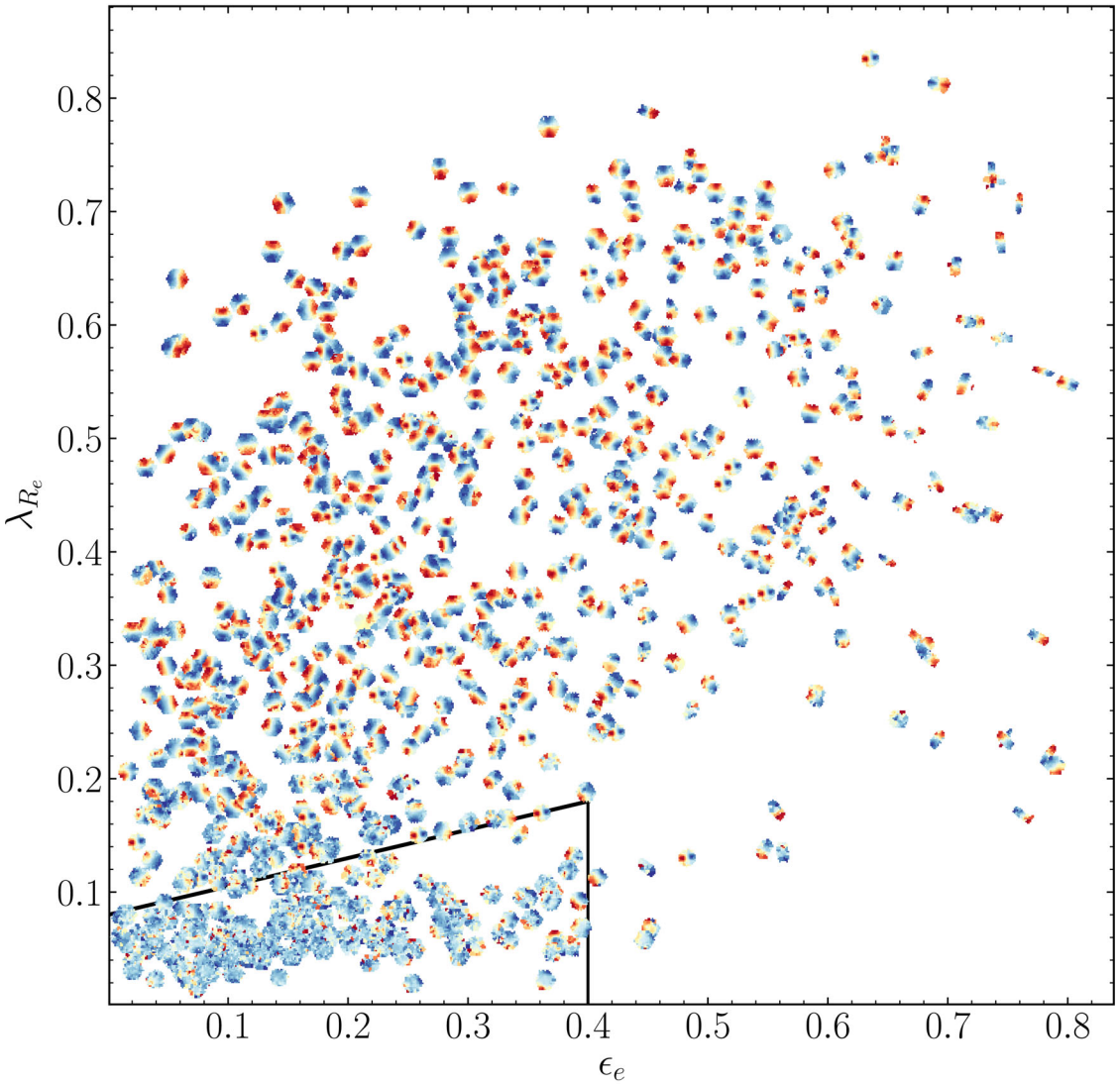

Figure 2. Ellipticity versus stellar angular momentum for the regular and non-regular rotators of the Q-MANGA-GALEX sample. Each point is shown by its stellar velocity map, each normalized to have a stellar velocity of 0 km s^{-1} shown by the colour yellow. We show the separation between regular (i.e. fast) and non-regular rotators (i.e. slow rotators and objects with kinematically decoupled cores) from Cappellari (2016) with the solid black line.

comparison is not possible, we can at least determine if the fraction of non-regular rotators in the Q-MANGA-GALEX sample is a sensible figure given previous estimates. Considering our sample is agnostic to visual morphology, we would expect this selection effect to dominate, resulting in a smaller fraction of non-regular rotators than previous works, which specifically derived the fraction of non-regular rotators in a sample of early-types only. However, many other studies have also shown that the non-regular rotator fraction increases with stellar mass (Cappellari et al. 2013), up to ∼90 per cent at 10^{12} M$_\odot$ (Veale et al. 2017). The median stellar mass of the Q-MANGA-GALEX sample is $10^{10.8}$ M$_\odot$, which is higher than the median stellar mass of the ATLAS^{3D} sample at $10^{10.5}$ M$_\odot$, likely accounting for this apparent discrepancy.

In order to obtain a sample of slow rotators, one author (RJS) inspected the velocity maps of the 168 non-regular rotators identified in the Q-MANGA-GALEX sample to remove those galaxies that showed rotation in their kinematic map (i.e. counter rotation or decoupled cores). A total of 71 galaxies exhibiting rotation were identified, example velocity maps for which are shown in the top row of Fig. 3. This resulted in a sample of 97 slow rotators, example velocity maps for which are shown in the middle row of Fig. 3.

In order to control for the degeneracies between mass, metallicity and dust (all of which can redden a galaxy's optical colour and mimic the effects of quenching), we selected a sub-sample of fast rotators from those identified as regular rotators in the Q-MANGA-GALEX sample. We matched to within ±2.5 per cent of the stellar mass of each slow rotator to give 97 fast rotators, example velocity maps for which are shown in the bottom row of Fig. 3. We shall refer to this combined sample of 194 fast and slow rotators as the MM-Q-MANGA-GALEX sample. An Anderson–Darling (AD; Anderson & Darling 1952) test reveals that the distribution of stellar masses of the fast rotators and slow rotators within this sample is statistically indistinguishable ($p = 0.22$). Similarly, their redshift distributions are also statistically indistinguishable ($p = 0.19$).

The optical and *NUV* colours from SDSS and *GALEX* (see Section 2.1) for the MM-Q-MANGA-GALEX sample are shown in Fig. 4. Performing AD tests on the distributions of the colours of the slow and fast rotators in the MM-Q-MANGA-GALEX sample reveals that both

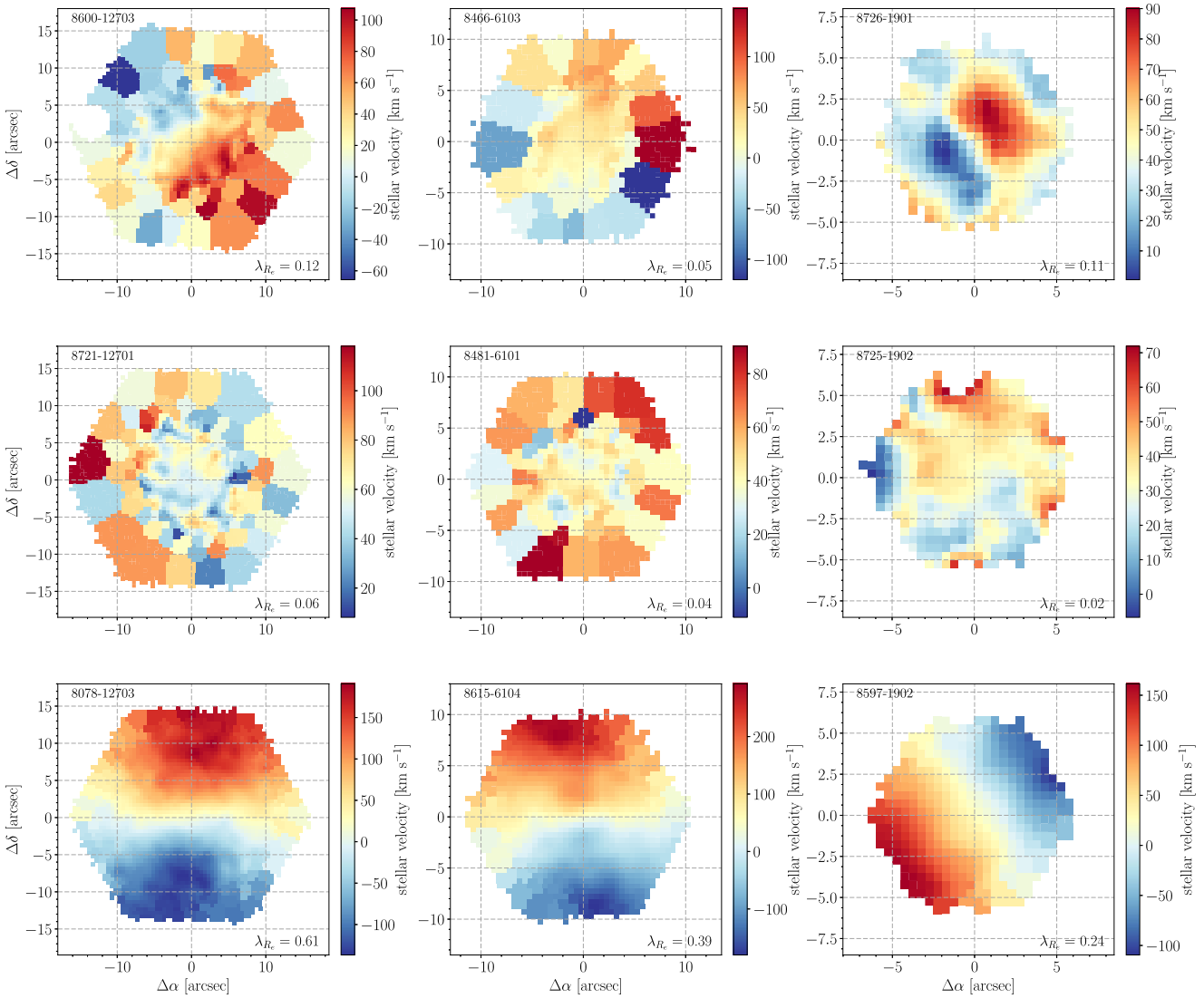

Figure 3. Example stellar velocity maps, Voronoi binned with a signal-to-noise ratio of 10, for three galaxies removed from the non-regular rotator Q-MANGA-GALEX sample because their kinematics show rotation (top row), three slow rotator galaxies without rotation (middle row) and three fast rotator galaxies with rotationally supported kinematics (bottom row). The MaNGA ID of each galaxy is shown in the top left-hand of each panel and the measured λ_{R_e} value in the bottom right-hand side. The number of spectral fibres in the MaNGA IFU bundle for each observation decreases from the left- to right-hand side.

the $u - r$ (AD = 5.9, $p = 0.002$) and $NUV - u$ (AD = 19.1, $p = 1 \times 10^{-5}$) colours of the two kinematic classifications are statistically distinguishable. These colours will be used to infer the SFHs of the MM-Q-MANGA-GALEX sample (see Section 2.6).

2.5 Environmental densities

We also consider the environmental densities of the fast and slow rotators by using estimates of the projected 5th nearest neighbour density, $\log \Sigma_5$, from Bamford et al. (2009). An AD test reveals that the distribution of environment densities of the 72 slow rotators and 80 fast rotators of the MM-Q-MANGA-GALEX sample with $\log \Sigma_5$ measurements from Bamford et al. (2009) is statistically indistinguishable ($p = 0.28$).

This is surprising since the current theory is that slow rotators are more likely to be the central galaxy of a group or cluster, whereas fast rotators are more likely to be satellite galaxies (Cappellari et al. 2011; D'Eugenio et al. 2013; Houghton et al. 2013; Scott et al. 2014). However, the MaNGA sample was chosen to be agnostic to galaxy environment, giving rise to a representative distribution of galaxy environments. Most galaxies in the sample will therefore reside in groups, a more common environment for a galaxy than the relatively rare environments of rich clusters (Carlberg 2004) or voids (Rieder et al. 2013). We must therefore probe the positions of the two samples within the group environment itself.

Cross-matching the MM-Q-MANGA-GALEX sample with the Yang, Mo & van den Bosch (2009) SDSS group catalogue gives us group information for 94 of the slow rotators and 96 of the fast rotators. Similar fractions of these slow, 75/94 (80 per cent), and fast rotators, 70/96 (73 per cent), are classified as their brightest group galaxy (BGG). However, these fractions include those galaxies that are isolated in their haloes (due to the theoretical definition of a BGG used in the Yang et al. 2009 catalogue). These isolated galaxies could be the remains of a fossil group (Ponman et al. 1994; Jones, Ponman & Forbes 2000; Jones et al. 2003) or could be truly isolated, at the opposite end of the evolutionary spectrum which we are trying

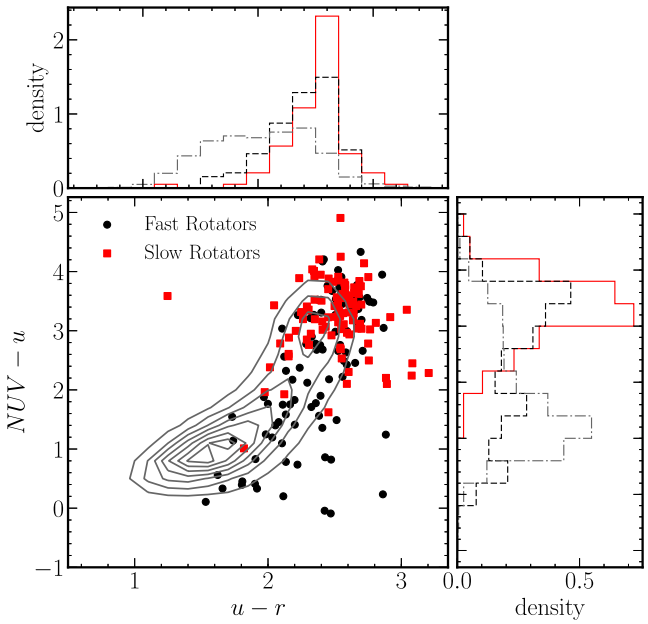

Figure 4. Colour–colour diagram showing the optical $u - r$ and $NUV - u$ colours of the fast (black circles) and slow (red squares) rotators of the MM-Q-MANGA-GALEX sample (main panel). Overlaid is the distribution of colours in a large SDSS–*GALEX* cross-matched sample from Smethurst et al. (2015) for reference (grey contours). The top panel shows the normalized distribution of the $u - r$ colours of the fast (black dashed) and slow (red solid) rotators of the MM-Q-MANGA-GALEX sample, along with the distribution for the Smethurst et al. (2015) sample for reference (grey dot–dashed). Similarly, the right-hand panel shows the normalized distribution of the $NUV - u$ colours of the fast (black dashed) and slow (red solid) rotators of the MM-Q-MANGA-GALEX sample, along with the distribution for the Smethurst et al. (2015) sample for reference (grey dot–dashed).

to probe. We must therefore remove these single galaxy 'groups' in order to properly test whether the slow rotators are preferentially found at the centre of the groups in the MM-Q-MANGA-GALEX sample.

Testing the distributions of the total group stellar mass for the fast and slow rotators, we find they are statistically distinguishable (AD test $p = 0.03$), with slow rotators residing in more massive groups. If we then consider only those galaxies in groups with a total stellar mass greater than 10^{11} $M_{\odot}$ (under the simplifying assumption that this will remove the majority of single galaxy 'groups'), we find the fraction of slow rotators classified as a BGG is 44/61 (72 per cent), whereas for fast rotators this drops to 30/52 (58 per cent), a statistically distinguishable difference ($p = 0.04$). Therefore, although the projected local environment densities of the two kinematic classes of galaxies are statistically indistinguishable, their positions within that given environment density do differ, as expected.

Given the above statistical tests, the only differences between the fast and slow rotators of the MM-Q-MANGA-GALEX sample are their kinematics, their colours and their position within their group halo.

2.6 Star formation history inference

STARPY[4] is a PYTHON code that allows the inference of the exponentially declining star formation history (SFH) of a single galaxy using Bayesian Markov chain Monte Carlo techniques (Foreman-Mackey et al. 2013)[5]. The code uses the solar metallicity stellar population models of Bruzual & Charlot (2003, hereafter BC03), assumes a Chabrier IMF (Chabrier 2003) and requires the input of the observed $u - r$ and $NUV - u$ colours and redshift. No attempt is made to model for intrinsic dust.

The SFH is described by an exponentially declining SFR described by two parameters; the time at the onset of quenching, t_q (Gyr), and the exponential rate at which quenching occurs, τ (Gyr). Under the simplifying assumption that all galaxies formed at $t = 0$ Gyr with an initial burst of star formation, the SFH can be described as

$$\mathrm{SFR} = \begin{cases} i_{\mathrm{sfr}}(t_q) & \text{if } t < t_q \\ i_{\mathrm{sfr}}(t_q) \times exp\left(\frac{-(t-t_q)}{\tau}\right) & \text{if } t > t_q \end{cases} \quad (3)$$

where i_{sfr} is an initial constant SFR dependent on t_q (Schawinski et al. 2014; Smethurst et al. 2015). The simplifying assumption that all galaxies formed at $t = 0$ Gyr means that the age of each galaxy, t_{age}, corresponds to the age of the Universe at its observed redshift, t_{obs}. A smaller τ value corresponds to a rapid quench, whereas a larger τ value corresponds to a slower quench. A galaxy undergoing a slow quench is not necessarily quiescent by the time of observation. This SFH model has previously been shown to appropriately characterize quenching galaxies (Weiner et al. 2006; Martin et al. 2007; Noeske et al. 2007; Schawinski et al. 2014).

The probabilistic fitting methods to these star formation histories for an observed galaxy are described in full detail in section 3.2 of Smethurst et al. (2015), wherein the STARPY code was used to characterize the morphologically dependence of the SFHs of ∼126 000 galaxies. Similarly, in Smethurst et al. (2016), STARPY was used to show the prevalence of rapid, recent quenching within a population of AGN host galaxies and in Smethurst et al. (2017) to investigate the quenching histories of group galaxies.

Briefly, we assume a flat prior on all the model parameters and model the difference between the observed and predicted $u - r$ and $NUV - u$ colours as independent realizations of a double Gaussian likelihood function (equation 2 in Smethurst et al. 2015). An example posterior probability distribution output by STARPY is shown for a single galaxy in fig. 5 of Smethurst et al. (2015), wherein the degeneracies of the SFH model between recent, rapid quenching and earlier, slower quenching can be seen.

To study the SFH across a sample of many galaxies, these individual posterior probability distributions are stacked in $[t_q, \tau]$ space to give one distribution across each quenching parameter for the sample. This is no longer inference but merely a method to visualize the results for a population of galaxies (see appendix section C in Smethurst et al. 2016 for a discussion on alternative methods that may be used to determine the parent population SFH). These distributions will be referred to as the population SFH densities.

3 RESULTS

We determine the population SFH densities for both the fast and slow rotators of the MM-Q-MANGA-GALEX sample. This is shown in Fig. 5 for both the onset time (left-hand panel) and exponential rate (right-hand panel) of quenching for the fast (black solid line) and slow (red dashed line) rotators. Uncertainties on the population densities (shown by the shaded regions) are determined from the maximum and minimum values spanned by $N = 1000$ bootstrap

[4] Publicly available: http://github.com/zooniverse/starpy

[5] http://dan.iel.fm/emcee/

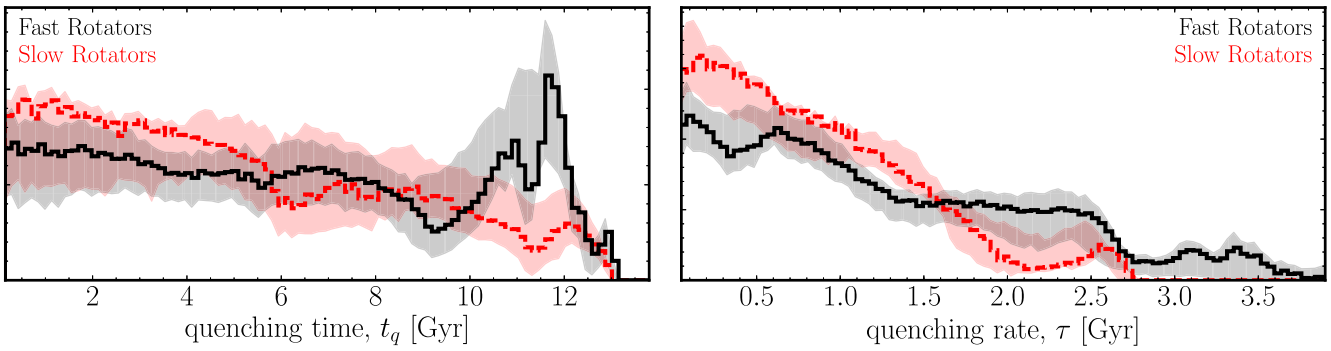

Figure 5. Population densities for the time, t_q (left-hand panel) and exponential rate, τ (right-hand panel) that quenching occurs in the MM-Q-MANGA-GALEX sample for the fast (black, solid) and slow (red, dashed) rotators. A high value of t_q corresponds to a recent quench, and a high value of τ corresponds to a slow quench. Shaded regions show the uncertainties on the distributions from bootstrapping.

iterations, each sampling 90 per cent of either the fast (black shaded region) or slow (red shaded region) rotators.

To statistically test the significance of our results, we estimate the 'best-fitting' $[t_q, \tau]$ values for each galaxy with the median value of an individual galaxy's posterior probability distribution from STARPY (i.e. the 50th percentile position of the MCMC chain). We test the distribution of these values of the fast and slow rotators in the MM-Q-MANGA-GALEX sample with AD tests. First, an AD test on the distributions of t_q values in the fast and slow rotator samples revealed that we cannot reject the null hypothesis that the fast and slow rotators quench at the same time (AD $= 0.65$, $p = 0.69$). Finally, an AD test on the distributions of τ values revealed that we can reject the null hypothesis that the fast and slow rotators quench at the same rate (AD $= 6.3$, $p = 0.001$). This is a 3.2σ result that suggests that slow rotators quench faster than fast rotators of the same mass.

4 DISCUSSION

The results presented in Section 3 suggest that fast and slow rotators are indeed separate populations quenched, and therefore formed, by different mechanisms. However, these quenching mechanisms occur at statistically indistinguishable onset times for fast and slow rotators. Khochfar et al. (2011) find in their simulations that the last major merger interaction for slow rotators was at $z \gtrsim 1.5$ (i.e. $t_q \lesssim 4.5$ Gyr). However, Penoyre et al. (2017) find in the Illustris simulation that slow rotators only form after $z < 1$ (i.e. $t_q \gtrsim 6$ Gyr). We note that STARPY is not very sensitive to the time of quenching, particularly at early times ($t_q \lesssim 6$ Gyr when $z \gtrsim 1$), due to the degeneracies between the optical and *NUV* colours currently used to infer the quenching parameters. Therefore, we cannot currently conclude which scenario our results favour. Future work altering our inference code to take spatial spectral information provided by MaNGA may help us to address this issue by breaking the degeneracies inherent in the photometric colours.

However, STARPY in its current form is sensitive to the rate of quenching in a galaxy. In the right-hand panel of Fig. 5, we see that there is a wide range of quenching rates occurring within the fast rotator sample. Previous works using STARPY have shown how the intermediate quenching rates $[1 \lesssim \tau \text{ (Gyr)} \lesssim 2]$ prevalent in the distribution of the fast rotator sample can be attributed to environmental processes such as harassment and galaxy interactions (Smethurst et al. 2017), or minor mergers (Smethurst et al. 2015). This is unsurprising given that the fast rotators are less likely to be the BGG than the slow rotators of the MM-Q-MANGA-GALEX sample, as discussed in Section 2.5.

In particular, we find evidence for galaxies in the fast rotator sample to quench at slow rates ($\tau \geq 2$ Gyr). Since the Q-MANGA-GALEX sample is agnostic to visual morphology, it will contain fast rotators that are disc-dominated (i.e. late-type galaxies). This preference for slow quenching rates is therefore likely to be caused by the effects of secular evolution through gas accretion and morphological quenching, slowly moving these disc galaxies off the SFS to produce the red spiral population of Masters et al. (2012). Using the morphological classifications of Galaxy Zoo 2 (GZ2 Lintott et al. 2011; Willett et al. 2013), we find that 20/97 (21 per cent) of the fast rotators of the MM-Q-MANGA-GALEX sample are disc dominated with a disc or featured debiased vote fraction, $p_d \geq 0.8$ (i.e. 80 per cent of classifiers marked the galaxy as having either a disc or features). This is consistent with the fact that $23 \pm^{2}_{11}$ per cent of the fast rotator quenching rate population density (black line in the right-hand panel of Fig. 5) is found at quenching rates $\tau > 2$ Gyr.

Conversely, only 1 of the slow rotators was classified as having a disc or features by GZ2[6] It is not surprising therefore that there is much less preference for slow quenching rates, with $\tau \geq 2$ Gyr, for slow rotators than fast rotators in the right-hand panel of Fig. 5. However, Smethurst et al. (2015) found for galaxies in the red sequence visually classified as 'smooth' in GZ2 (i.e. quenching or quenched early-types) that a significant fraction, 26.1 per cent, of the quenching rate population density was found at these slow quenching rates (see the left-hand panel of their fig. 8). However, a sample of visually classified 'smooth' galaxies in GZ2 may include both fast and slow rotators. It is only in this work that we have been able to investigate the difference in the SFHs of galaxies that are rotationally supported from those that are not, revealing that the stellar kinematics are driving the morphologically dependant star formation histories seen in Smethurst et al. (2015).

The slow rotators in the MM-Q-MANGA-GALEX sample instead show a preference for rapid quenching rates ($\tau \lesssim 1$ Gyr) in the right-hand panel of Fig. 5. Assuming that major mergers are the only mechanism able to destroy rotation in a galaxy, this result supports the theory that these galaxies are formed by major mergers that, along with destroying the disc of a galaxy, are thought to cause quenching at such rapid rates (Springel, Di Matteo & Hernquist 2005; Bell et al. 2006; Lotz et al. 2008, 2011). Surprisingly, we also find

[6] Upon visual inspection, this galaxy has a large disc with spiral structure lying outside of the MaNGA fibre bundle at > 1.5 R_e.

evidence that some of the fast rotators are quenching at these same rapid rates ($\tau \lesssim 1$ Gyr) in the right-hand panel of Fig. 5. This suggests that in a fraction of fast rotators, a dynamically fast process, such as a major merger, may be the cause of quenching.

Simulations have recently shown that although major mergers (2:1 or 1:1 mergers) can cause rapid quenching of a galaxy, they do not necessarily destroy the disc-dominated nature of a galaxy (Pontzen et al. 2016; Sparre & Springel 2016) and can actually form a fast rotator remnant (Bois et al. 2011). This is thought to mainly occur in gas rich major mergers (Bois et al. 2011) and is likely the explanation for the presence of rapid rates in the fast rotator sample seen in the right-hand panel of Fig. 5. We therefore predict that the fast rotators in the MM-Q-MANGA-GALEX sample will be more gas rich than the slow rotators they are stellar mass matched to. We will be able to test this hypothesis with currently ongoing follow-up observations using the Green Bank Telescope (GBT16A-095 and GBT17A-012; Masters et al. in preparation) which will obtain H I profiles for galaxies in the MaNGA target sample. With these observations, we will be able to determine whether gas mass has an impact on the formation mechanisms of these kinematically distinct galaxies.

5 CONCLUSIONS

We have investigated the star formation histories of quenching or quenched fast and slow rotators identified in the MaNGA galaxy sample, irrespective of their visual morphology. We used the $u - r$ and $NUV - u$ colours with an existing piece of inference software, STARPY, to determine the onset time and exponential rate of quenching in each of these galaxies.

An Anderson–Darling test revealed that the distribution of the inferred quenching rates of fast and slow rotators is statistically distinguishable ($p = 0.001$, 3.2σ). We find that rapid quenching rates ($\tau \lesssim 1$ Gyr) are dominant for slow rotators, supporting the theory that slow rotators form in dynamically fast processes, such as major mergers (Bois et al. 2010; Duc et al. 2011; Naab et al. 2014). Conversely, we find that fast rotators quench at a wide range of rates, consistent with dynamically slow processes such as secular evolution, minor mergers, gas accretion and environmentally driven mechanisms. However, we also find evidence that some of the fast rotators are quenching at the same rapid rates dominant across the slow rotator sample.

This finding of rapid quenching rates occurring for both slow rotators and a subset of the fast rotators suggests that although their kinematics are different in nature, both classes of galaxy may be able to quench, and therefore form, via major mergers. This result combined with the findings of recent simulations showing disc survival in gas-rich major mergers (Bois et al. 2011; Pontzen et al. 2016; Sparre & Springel 2016) suggests that the total gas mass fraction within a pair of merging galaxies is what will ultimately decide the kinematic fate of a galaxy.

ACKNOWLEDGEMENTS

RJS gratefully acknowledges research funding from the Ogden Trust. AW acknowledges support of a Leverhulme Trust Early Career Fellowship.

Based on observations made with the NASA Galaxy Evolution Explorer. *GALEX* is operated for NASA by the California Institute of Technology under NASA contract NAS5-98034.

Funding for the Sloan Digital Sky Survey IV has been provided by the Alfred P. Sloan Foundation, the U.S. Department of EnergyOffice of Science and the Participating Institutions. SDSS acknowledges support and resources from the Center for High-Performance Computing at the University of Utah. The SDSS web site is www.sdss.org.

SDSS is managed by the Astrophysical Research Consortium for the Participating Institutions of the SDSS Collaboration including the Brazilian Participation Group, the Carnegie Institution for Science, Carnegie Mellon University, the Chilean Participation Group, the French Participation Group, Harvard-Smithsonian Center for Astrophysics, Instituto de Astrofísica de Canarias, The Johns Hopkins University, Kavli Institute for the Physics and Mathematics of the Universe (IPMU) / University of Tokyo, Lawrence Berkeley National Laboratory, Leibniz Institut für Astrophysik Potsdam (AIP), Max-Planck-Institut für Astronomie (MPIA Heidelberg), Max-Planck-Institut für Astrophysik (MPA Garching), Max-Planck-Institut für Extraterrestrische Physik (MPE), National Astronomical Observatories of China, New Mexico State University, New York University, University of Notre Dame, Observatório Nacional / MCTI, The Ohio State University, Pennsylvania State University, Shanghai Astronomical Observatory, United Kingdom Participation Group, Universidad Nacional Autónoma de México, University of Arizona, University of Colorado Boulder, University of Oxford, University of Portsmouth, University of Utah, University of Virginia, University of Washington, University of Wisconsin, Vanderbilt University and Yale University.

REFERENCES

Abazajian K. N. et al., 2009, ApJS, 182, 543
Abolfathi B. et al., 2017, preprint (arXiv:e-prints)
Aguerri J. A. L., González-García A. C., 2009, A&A, 494, 891
Anderson T. W., Darling D. A., 1952, Ann. Math. Statist., 23, 193
Bamford S. P. et al., 2009, MNRAS, 393, 1324
Bell E. F., Phleps S., Somerville R. S., Wolf C., Borch A., Meisenheimer K., 2006, ApJ, 652, 270
Blanton M. R., Roweis S., 2007, AJ, 133, 734
Blanton M. R., Eisenstein D., Hogg D. W., Schlegel D. J., Brinkmann J., 2005, ApJ, 629, 143
Blanton M. R. et al., 2017, AJ, 154, 28
Bois M. et al., 2010, MNRAS, 406, 2405
Bois M. et al., 2011, MNRAS, 416, 1654
Brinchmann J., Charlot S., White S. D. M., Tremonti C., Kauffmann G., Heckman T., Brinkmann J., 2004, MNRAS, 351, 1151
Bruzual G., Charlot S., 2003, MNRAS, 344, 1000
Bundy K. et al., 2015, ApJ, 798, 7
Cappellari M., 2016, ARA&A, 54, 597
Cappellari M., Copin Y., 2003, MNRAS, 342, 345
Cappellari M., Emsellem E., 2004, PASP, 116, 138
Cappellari M. et al., 2007, MNRAS, 379, 418
Cappellari M. et al., 2011, MNRAS, 413, 813
Cappellari M. et al., 2013, MNRAS, 432, 1862
Cardelli J. A., Clayton G. C., Mathis J. S., 1989, ApJ, 345, 245
Carlberg R. G., 2004, in Mulchaey J. S., Dressler A., Oemler A., eds, Clusters of Galaxies: Probes of Cosmological Structure and Galaxy Evolution. Cambridge Univ. Press, Cambridge, p. 343
Chabrier G., 2003, PASP, 115, 763
Croton D. J. et al., 2006, MNRAS, 365, 11
D'Eugenio F., Houghton R. C. W., Davies R. L., Dalla Bontà E., 2013, MNRAS, 429, 1258
Drory N. et al., 2015, AJ, 149, 77
Duc P.-A. et al., 2011, MNRAS, 417, 863
Emsellem E. et al., 2007, MNRAS, 379, 401
Emsellem E. et al., 2011, MNRAS, 414, 888
Fang J. J., Faber S. M., Koo D. C., Dekel A., 2013, ApJ, 776, 63

Foreman-Mackey D., Hogg D. W., Lang D., Goodman J., 2013, PASP, 125, 306
Gunn J. E. et al., 2006, AJ, 131, 2332
Hayward C. C., Torrey P., Springel V., Hernquist L., Vogelsberger M., 2014, MNRAS, 442, 1992
Hopkins P. F., Hernquist L., Cox T. J., Kereš D., 2008, ApJS, 175, 356
Houghton R. C. W. et al., 2013, MNRAS, 436, 19
Jarosik N. et al., 2011, ApJS, 192, 14
Johnston E. J., Aragón-Salamanca A., Merrifield M. R., 2014, MNRAS, 441, 333
Jones L. R., Ponman T. J., Forbes D. A., 2000, MNRAS, 312, 139
Jones L. R., Ponman T. J., Horton A., Babul A., Ebeling H., Burke D. J., 2003, MNRAS, 343, 627
Kauffmann G. et al., 2003, MNRAS, 341, 33
Khochfar S. et al., 2011, MNRAS, 417, 845
Knebe A., Power C., Gill S. P. D., Gibson B. K., 2006, MNRAS, 368, 741
Law D. R. et al., 2015, AJ, 150, 19
Law D. R. et al., 2016, AJ, 152, 83
Lintott C. et al., 2011, MNRAS, 410, 166
Lotz J. M., Jonsson P., Cox T. J., Primack J. R., 2008, MNRAS, 391, 1137
Lotz J. M., Jonsson P., Cox T. J., Croton D., Primack J. R., Somerville R. S., Stewart K., 2011, ApJ, 742, 103
Martig M., Bournaud F., Teyssier R., Dekel A., 2009, ApJ, 707, 250
Martin D. C. et al., 2005, ApJ, 619, L1
Martin D. C. et al., 2007, ApJS, 173, 342
Masters K. L. et al., 2012, MNRAS, 424, 2180
Naab T. et al., 2014, MNRAS, 444, 3357
Noeske K. G. et al., 2007, ApJ, 660, L43
Oh K., Sarzi M., Schawinski K., Yi S. K., 2011, ApJS, 195, 13
Padmanabhan N. et al., 2008, ApJ, 674, 1217
Peng Y.-j. et al., 2010, ApJ, 721, 193
Peng Y.-j., Lilly S. J., Renzini A., Carollo M., 2012, ApJ, 757, 4
Penoyre Z., Moster B. P., Sijacki D., Genel S., 2017, MNRAS, 468, 3883
Ponman T. J., Allan D. J., Jones L. R., Merrifield M., McHardy I. M., Lehto H. J., Luppino G. A., 1994, Nature, 369, 462
Pontzen A., Tremmel M., Roth N., Peiris H. V., Saintonge A., Volonteri M., Quinn T., Governato F., 2016, MNRAS, 465, 547
Rieder S., van de Weygaert R., Cautun M., Beygu B., Portegies Zwart S., 2013, MNRAS, 435, 222
Schawinski K. et al., 2014, MNRAS, 440, 889
Scott N., Davies R. L., Houghton R. C. W., Cappellari M., Graham A. W., Pimbblet K. A., 2014, MNRAS, 441, 274
SDSS Collaboration et al., 2016, preprint (arXiv:e-prints)
Sheth K., Vogel S. N., Regan M. W., Thornley M. D., Teuben P. J., 2005, ApJ, 632, 217
Smee S. A. et al., 2013, AJ, 146, 32
Smethurst R. J. et al., 2015, MNRAS, 450, 435
Smethurst R. J. et al., 2016, MNRAS, 463, 2986
Smethurst R. J., Lintott C. J., Bamford S. P., Hart R. E., Kruk S. J., Masters K. L., Nichol R. C., Simmons B. D., 2017, MNRAS, 469, 3670
Snyder G. F., Cox T. J., Hayward C. C., Hernquist L., Jonsson P., 2011, ApJ, 741, 77
Somerville R. S., Hopkins P. F., Cox T. J., Robertson B. E., Hernquist L., 2008, MNRAS, 391, 481
Sparre M., Springel V., 2016, MNRAS, 470, 3946
Springel V., Di Matteo T., Hernquist L., 2005, ApJ, 620, L79
Stott J. P. et al., 2016, MNRAS, 457, 1888
Stoughton C. et al., 2002, AJ, 123, 485
Toloba E. et al., 2015, ApJ, 799, 172
Toomre A., Toomre J., 1972, ApJ, 178, 623
Veale M. et al., 2017, MNRAS, 464, 356
Wake D. A. et al., 2017, AJ, 154, 26
Weiner B. J. et al., 2006, ApJ, 653, 1049
Willett K. W. et al., 2013, MNRAS, 435, 2835
Yan R. et al., 2016, AJ, 152, 197
Yang X., Mo H. J., van den Bosch F. C., 2009, ApJ, 695, 900
York D. G. et al., 2000, AJ, 120, 1579
Zurita A., Relaño M., Beckman J. E., Knapen J. H., 2004, A&A, 413, 73

This paper has been typeset from a TEX/LATEX file prepared by the author.